arXiv:1405.1315v1 [physics.ao-ph] 6 May 2014

Deep ocean early warning signals of an Atlantic MOC collapse

Qing Yi Feng, Jan P. Viebahn and Henk A. Dijkstra

Institute for Marine and Atmospheric research Utrecht (IMAU),
Department of Physics and Astronomy, Utrecht University, Utrecht, The Netherlands.

The Atlantic Meridional Overturning Circulation (MOC) is a crucial part of the climate system because of its associated northward heat transport [1, 2]. The present-day MOC is sensitive to freshwater anomalies and may collapse to a state with a strongly reduced northward heat transport [3, 4]. A future collapse of the Atlantic MOC has been identified as one of the most dangerous tipping points in the climate system [7]. It is therefore crucial to develop early warning indicators for such a potential collapse based on relatively short time series. So far, attempts to use indicators based on critical slowdown have been marginally successful [8]. Based on complex climate network reconstruction [9, 10], we here present a promising new indicator for the MOC collapse that efficiently monitors spatial changes in deep ocean circulation. Through our analysis of the performance of this indicator we formulate optimal locations of measurement of the MOC to provide early warning signals of a collapse. Our results imply that an increase in spatial resolution of the Atlantic MOC observations (i.e., at more sections) can improve early detection, because the spatial coherence in the deep ocean arising near the transition is better captured.

To develop this indicator and to study its performance, we use the results from the control simulation and the freshwater perturbed (from now on referred to as 'hosing') simulation of the FAMOUS climate model (see Methods). In the hosing simulation, the freshwater flux over the extratropical North Atlantic is increased linearly from zero to 1.0 Sv (1 Sv = 10^6 m^3s^{-1}) over 2000 years [11]. Fig. 1**a** displays the annual mean time series of the Atlantic MOC value at latitude 26°N and at 1000 m depth for the control simulation (green curve) and the hosing simulation (blue curve). Whereas the control MOC values are statistically stationary over the 2000 year integration period, the MOC values for the hosing simulation show a rapid decrease between the years 800-1050.

We also use results from the FAMOUS simulations in which the freshwater flux was fixed after a certain integration time and the model was integrated to equilibrium [11]. Time series of the MOC of the last 100 years of these simulations were analyzed and the mean MOC values (again at 26°N and 1000 m depth) are plotted as the red dots labeled from 1 to 6 in Fig. 1**a**. Figure 1**b-d** show mean MOC streamfunction patterns of three of these equilibrium simulations (labelled with 1, 4 and 6 in Fig. 1**a**). Although the equilibrium value of the MOC decreases with larger freshwater inflow, the changes in the MOC pattern are relatively minor.

For a slightly higher value of the freshwater flux as at point 6, the equilibrium solution is already a collapsed state [11]. In the hosing simulation, the freshwater is, however, added relatively fast compared to the equilibration time scale of the MOC. Hence the MOC maintains its pattern for much higher freshwater inflow and collapses near year 900 (Fig. 1**a**). To determine a collapse time τ_c more precisely, we use the control simulation of FAMOUS (see Methods). We find $\tau_c = 874$ years and τ_c is shown as the red dashed line in Fig. 1**a**.

Critical slowdown has been a key phrase in the detection of tipping points in ecosystems [12] and the climate system [8]. Indeed in many natural and man-made systems, there is an increase in response times to perturbations as a tipping point is approached [13]. The detection of MOC collapses and the design of early warning signals has so far mostly been based on the analysis of single time series [14, 8]. Critical slowdown induces changes in variance and lag-1 autocorrelation in the time series that can be connected to the distance to the tipping point and hence these quantities can serve as early warning indicators [13].

Here we build on an idea to use complex network theory to construct an early warning indicator [15]. The complex network we employ in this study is the Pearson Correlation Climate Network [17] abbreviated below as PCCN (see Methods for details on the network reconstruction). We first construct PCCNs using the complete Atlantic MOC field for each of the six 100 year equilibrium simulations (red dots in Fig. 1**a**). For the topological analysis of the PCCNs, we only use the degree field [9, 10, 18]. The degree of a node is the number of links between this node and other nodes. As shown in Fig. 2 the changes in the degree field at the equilibrium solutions 1, 2, 4 and 6 in Fig. 1**a** are distinct. When the freshwater forcing is increased, high degree in the network – indicating high spatial MOC correlations – first appears at nodes in the South Atlantic at about 1000 m depth (Fig. 2**a-b**).

It subsequently extends to the whole Atlantic with highest amplitudes in the deep ocean at midlatitudes (Fig. 2**c-d**).

A similar result was obtained using networks from the temperature field of an idealized spatially two-dimensional model of the MOC [15]. The behavior of the degree field can be understood from the underlying structure of the Empirical Orthogonal Functions (EOFs) of the MOC field (see Supplementary Information). Once the transition is approached, one of the EOFs becomes most dominant in the variability. The network can be seen as a coarse-graining of the variability and by focussing only on the largest correlations, it is ideally suited to monitor the changes in spatial correlations of the system once the transition is approached.

Next, we study the transient behavior of the hosing simulation by constructing similar PCCNs (see Methods for details on the sliding window and threshold values τ used). In [15], the kurtosis K_d of the degree distribution was introduced as an effective indicator to capture the changes in the topology of the degree field. For the complete Atlantic MOC field, the values of K_d for the hosing simulation (blue curve) and for the control simulation (green curve) are plotted in Fig. 3**a**. For the hosing simulation, there is indeed a strong increase of K_d to values far extending those for the control simulation significantly before the collapse time τ_c. For comparison, the critical slowdown indicators variance (Fig. 3**b**) and lag-1 autocorrelation (Fig. 3**c**) based on the complete Atlantic MOC data (and using the same sliding window) do not show any early warning signal of the MOC transition before the collapse time τ_c.

To provide a measure of the performance of an indicator I, we introduce an evaluation scheme (see Methods), which consists of the detection time, the reliability of the indication, and the intensity of the indication, γ^I. The excellent performance of the kurtosis indicator K_d (with a detection time at 738 years, no false alarm and a positive value of γ^{K_d}) in Fig. 3**a** is shown in entry No.1 in Table 1.

So far, we used the complete Atlantic MOC field of the FAMOUS model data, but at the moment, MOC observations are only routinely made at 26°N through the RAPID-MOCHA program [19]. There are also initiatives to monitor the MOC at 35°S (SAMOC, see www.aoml.noaa.gov/phod/SAMOC_international) and at about 60°N (OSNAP, see www.o-snap.org). Motivated by the fact that current and near future available observations of the MOC will only be available along zonal sections in the Atlantic, we next reconstructed networks (and the indicator

K_d) from limited section MOC data of the FAMOUS model results.

The performance of the kurtosis indicator K_d for different sections and combinations of sections is shown in Table 1. The indicator K_d provides two false alarms (see Methods) and one relatively late alarm for data at 26°N (No. 2 in Table 1), no alarm at all for data at 33°S (No. 3 in Table 1) and does not perform well for all other single section data (see Supplementary Table 1). When the lag-1 autocorrelation and variance of time series averaged over a single section are considered (see Supplementary Tables 2 and 3), the lag-1 autocorrelation performs best at 21°N although it still gives a false alarm. The variance indicator does not give any warning for all single sections.

To determine the optimal observation locations of the MOC using K_d, we systematically deleted sections from the complete Atlantic MOC field and evaluated the performance of the indicator K_d for the remaining sections. Entry No. 4 in Table 1 shows that the indicator K_d still works well for the Atlantic MOC field with halved horizontal resolution (21(depth) $\times$ 21(latitude)= 441 nodes), as well as for the sets of sections including midlatitudes both in the Northern and Southern Hemisphere (No. 6-8 in Table 1). However, detection fails for the set of sections located only in the Northern Hemisphere at mid- and high latitudes (No. 5 in Table 1).

For the latitude sets I and II, consisting of 18°S, 13°S, 8°S, 11°N, 16°N, 21°N, 26°N and 31°N (blue curve in Fig. 4 and No. 9 in Table 1) or 33°S, 18°S, 13°S, 11°N, 16°N, 21°N, 26°N and 31°N (green curve in Fig. 4 and No. 10 in Table 1), respectively, the performance of the indicator K_d is comparable to the case of the complete Atlantic MOC field (Fig. 3**a** and No. 1 in Table 1). Both sets consist of 21(depth)$\times$8(latitude)= 168 grid points and hence are considerably reduced (by 81%) in comparison to the complete Atlantic MOC field. Further analysis (see Supplementary Table 4) indicates that the data at the sections 18°S and 31°N are essential for a good detection of the MOC collapse. The results of No. 9 and 10 in Table 1 also indicate that including the MOC data at 33°S (near the SAMOC section) would advance the detection time of a future collapse of the MOC compared to including a section at 8°S, but the detection intensity γ^{K_d} of the kurtosis indicator K_d slightly decreases.

The physical reason for the optimal observation regions is the following. In ocean-climate models, the MOC collapse is due to a robust feedback involving the transport of salinity by the ocean circulation, the salt-advection feedback [5, 6]. The subtropics are strong evaporation regions and hence the largest salinity gradients, central in the salt-advection feedback, are located

in these regions. Consequently, it is expected that here the strongest response due to the salt-advection feedback appears and hence the strongest spatial correlations in the MOC field. Support for this comes from the structure of the dominant EOFs of the equilibrium solutions where the largest amplitude is also located in these midlatitude regions (see Supplementary Material).

Using techniques of complex network theory we have provided a novel indicator which can give an early warning signal for a collapse of the MOC. When applied to data from the FAMOUS model [11], our results show that when the appropriate midlatitude North and South Atlantic MOC data are available, the kurtosis indicator K_d provides a strong anomalous signal at least 100 years before the transition. Although at the moment a collapse of the MOC is considered a high-impact but low-probability event [20], modesty is required regarding our confidence in this statement. The processes controlling the behavior of the MOC, such as the downwelling in the northern North Atlantic boundary currents, are not well represented in many of the climate models on which this statement is based. In state-of-the-art GCMs, such as those used in the IPCC AR5, MOC collapses have not been found yet but it is fair to say that these models have not been extensively tested for this behavior [20, 21].

Up to now, there is about 10 years of data on the MOC from the RAPID-MOCHA array, and although this array will likely be operational up to the year 2020, the temporal extend of the time series proceeds only slowly. Due to this insufficient length of the observational record, the indicator K_d is not yet applicable to observational data and hence cannot be used to determine whether the recent downward trend in the observed MOC strength at 26°N [22] is the start of a collapse. Such MOC behavior may just be related to natural variability such as that associated with the Atlantic Multidecadal Oscillation [23, 24]. The strong element of an indicator such as K_d is, however, that it is based in spatial correlations. Our results indicate that an increase in spatial resolution of the MOC observations (i.e., at more sections) can improve early detection using this indicator, because the spatial coherence arising near the transition is better captured. This is another reason that such observations should be given high priority in climate research.

Methods

Model: The FAMOUS model is a version of the HadCM3 model with a lower resolution ocean and atmosphere component; the details of the model are described in [11]. The model has horizontal resolution of $2.5^\circ \times 3.75^\circ$ and a vertical resolution of 20 levels. Annual mean data of the MOC field were analyzed for each simulation.

Collapse Time τ_c: With a Student t-test we first determine the time, say τ_s, at which the trend of the MOC time series of the hosing simulation deviates significantly (p = 0.05) from that of the control simulation. Subsequently, the standard deviation σ of the MOC values of the control simulation over the first τ_s years is computed. Next, the first time when the MOC anomaly value (with respect to the mean of the first τ_s years) in the hosing simulation decreases below - 3σ, we consider the MOC to start collapsing which defines τ_c. In the FAMOUS model, when considering the MOC values at 26°N and 1000 m depth, we find $\tau_s = 350$ years and $\tau_c = 874$ years.

Network Reconstruction: From the MOC data of the FAMOUS model over the latitudinal domain [35°S-70°N] of the Atlantic Ocean, we construct a Climate Network (CN). The nodes of the network are the latitude-depth values of the grid points of the model. A 'link' between two nodes is determined by a significant interdependence between their MOC anomaly time series. There are several measures of quantifying the degree of statistical interdependence, and the most common one is calculating the Pearson correlations of pairs of time series [16]. More precisely, in a Pearson Correlation Climate Network (PCCN) [17] an unweighted and undirected link between two nodes exists if the linear Pearson correlation coefficient of the MOC time series at these two nodes exceeds a threshold value such that the correlation is significant (p=0.05).

For example, in case of the complete Atlantic MOC field and the 100 year equilibrium simulations, each network consists of 21(depth) $\times$ 42 (latitude)= 882 nodes, and a threshold value of $\tau = 0.5$ guarantees that a Pearson correlation between MOC time series at two nodes exceeding τ is significant. For the hosing simulation, as shown in Fig. 1**a**, the MOC values display a significant trend which would affect the accuracy

of early warning signal detection. Hence, for the study of the transient behaviour of the hosing simulation, we first linearly detrend the MOC field before reconstruction of the PCCNs. Next, a 100-year sliding window size (with a shift of one year) is used and values of τ between 0.5 and 0.9 are chosen for each PCCN, which guarantees significant correlations (p = 0.05) in defining the links among the nodes in each PCCN.

Evaluation Scheme for the Performance of an Indicator:
1) *Detection time*: When a value of an indicator for the hosing simulation exceeds the maximum of the same indicator for the control simulation, we flag an alarm of a collapse. For example, the maximum of K_d for the control simulation (green curve in Fig. 3**a**) is plotted as the blue dashed line in Fig. 3**a**. In this case, an early warning signal is detected at year 738 which is 136 years before the MOC collapse time $\tau_c = 874$ years.
2) *False Alarm*: We label a detection time which is smaller than $\tau_c - 300$ years as a false alarm. The 300 years is based on the horizon considered in IPCC-AR5 [20] for the evolution of the climate system (such as reflected in the Extended Concentration Pathway Emissions and Forcing scenarios, ECPs). Such a time period is also considered to be a political time horizon [7] such that decisions taken within this period are able to affect the occurrence of a collapse. In addition, when the detection time is within $[\tau_c - 300, \tau_c]$, but the signal only lasts less than 5 years it is also considered as a false alarm.
3) *Detection intensity* γ^I: The amplitude of the peak of the indicator is also important. Therefore, we additionally define another quality measure γ^I for indicator I as

$$\gamma^I = \frac{\max_P(I^{hosing})}{\max_{[0,\tau_c]}(I^{control})} - 1$$

Here the maximum of the control is taken over the total time interval $[0, \tau_c]$ and that of the hosing only over the peak interval P where the indicator extends over the threshold value. The larger the value of γ^I the better the quality of the indicator I; if $\gamma^I \leq 0$ no detection occurs. For example, based on the results in Fig. 3**a** the value of γ^{K_d} for the complete Atlantic MOC field is about 0.07 (see No. 1 in Table 1).

Values of γ for both the variance (Fig. 3**b**) and the lag-1 autocorrelation (Fig. 3**c**) are smaller than zero.

Correspondence

Correspondence and requests for materials should be addressed to Q. Y. Feng (email: Q.Feng@uu.nl).

Author contribution

All three authors designed the study, Q. Y. Feng performed most of the analysis, and all authors contributed to the writing of the paper.

Acknowledgments

We thank Ed Hawkins and Robin Smith for providing the FAMOUS data and Jonathan Donges, Norbert Marwan and Reik Donner (PIK, Potsdam) for providing the software package "pyUnicorn" used in the network calculations here. The authors would like to acknowledge the support of the LINC project (no. 289447) funded by the Marie-Curie ITN program (FP7-PEOPLE-2011-ITN) of EC. QYF also thanks all the LINC members for constructive suggestions and technical support.

References

[1] Ganachaud, A. & Wunsch, C. Improved estimates of global ocean circulation, heat transport and mixing from hydrographic data. Nature **408**, 453–457 (2000).

[2] Johns, W., Baringer, M. & Beal, L. Continuous, array-based estimates of Atlantic Ocean heat transport at 26.5 N. Journal Of Climate **24**, 2429–2449 (2011).

[3] Bryan, F. O. High-latitude salinity effects and interhemispheric thermohaline circulations. Nature **323**, 301–304 (1986).

[4] Rahmstorf, S. The thermohaline circulation: a system with dangerous thresholds? Climatic Change **46**, 247–256 (2000).

[5] Stommel, H. Thermohaline convection with two stable regimes of flow. Tellus **2**, 244–230 (1961).

[6] Walin, G. The thermohaline circulation and the control of ice ages. Paleogeogr. Paleoclim. Paleoecol. **50**, 323–332 (1985).

[7] Lenton, T. M. et al. Tipping elements in the earth's climate system. Proceedings of the National Academy of Sciences **105**, 1786–1793 (2008).

[8] Lenton, T. M. Early warning of climate tipping points. Nature Publishing Group **1**, 201–209 (2011).

[9] Tsonis, A. A. & Swanson, K. L. What do networks have to do with climate? Bulletin Of The American Meteorological Society **87**, 585–595 (2006).

[10] Donges, J. F., Zou, Y., Marwan, N. & Kurths, J. Complex networks in climate dynamics. The European Physical Journal Special Topics **174**, 157–179 (2009).

[11] Hawkins, E. et al. Bistability of the Atlantic overturning circulation in a global climate model and links to ocean freshwater transport. Geophysical Research Letters **38**, L10605 (2011).

[12] Dakos, V., Kéfi, S., Rietkerk, M., van Nes, E. H. & Scheffer, M. Slowing down in spatially patterned ecosystems at the brink of collapse. The American Naturalist **177**, 154–166 (2011).

[13] Scheffer, M., Bascompte, J., Brock, W. A. & Brovkin, V. Early-warning signals for critical transitions. Nature **461**, 53–59 (2009).

[14] Livina, V. N. & Lenton, T. M. A modified method for detecting incipient bifurcations in a dynamical system. Geophysical Research Letters **34** (2007).

[15] Mheen, M. et al. Interaction network based early warning indicators for the Atlantic MOC collapse. Geophysical Research Letters **40**, 2714–2719 (2013).

[16] Tsonis, A. A. & Roebber, P. J. The architecture of the climate network. Physica A: Statistical Mechanics and its Applications **333**, 497–504 (2004).

[17] Feng, Q. Y. & Dijkstra, H. Are North Atlantic multidecadal SST anomalies westward propagating? Geophysical Research Letters **41**, 541–546 (2014).

[18] Viebahn, J. & Dijkstra, H. A. Critical Transition Analysis of the Deterministic Wind-Driven Ocean Circulation — A Flux-Based Network Approach. International Journal of Bifurcation and Chaos **24**, 1430007 (2014).

[19] Cunningham, S. A. et al. Temporal Variability of the Atlantic Meridional Overturning Circulation at 26.5 N. Science **317**, 935–938 (2007).

[20] Collins, M. et al. Long-term Climate Change: Projections, Commitments and Irreversibility. In Stocker, T. et al. (eds.) Climate Change 2013: The Physical Science Basis. Contribution of Working Group I to the F 1029–1136 (Cambridge: University of Cambridge Press Syndicate., UK, 2013).

[21] Huisman, S. E., den Toom, M., Dijkstra, H. A. & Drijfhout, S. An Indicator of the Multiple Equilibria Regime of the Atlantic Meridional Overturning Circulation. Journal Of Physical Oceanography **40**, 551–567 (2010).

[22] Smeed, D. A. et al. Observed decline of the atlantic meridional overturning circulation 2004 to 2012. Ocean Science Discussions **10**, 1619–1645 (2013). URL `http://www.ocean-sci-discuss.net/10/1619/2013/`.

[23] Kerr, R. A. A North Atlantic climate pacemaker for the centuries. Science **288**, 1984–1986 (2000).

[24] Knight, J. R., Allan, R. J., Folland, C. K., Vellinga, M. & Mann, M. E. A signature of persistent natural thermohaline circulation cycles in observed climate. Geophysical Research Letters **32**, L20708 (2005).

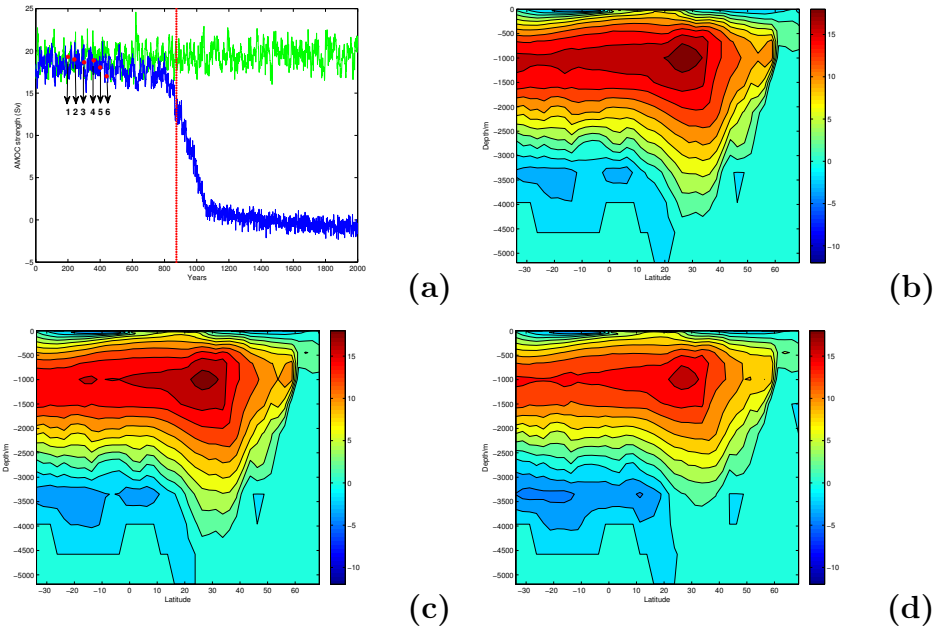

Figure 1: ***(a)*** *Time series of the MOC (in Sv, 1 Sv = 10^6 $m^3 s^{-1}$) at 26°N and 1000m depth in the Atlantic for the control simulation (green curve) and the freshwater perturbed simulation (blue curve) of the FAMOUS model. The red dots labeled from 1 to 6 show the average values of MOC from the corresponding equilibrium simulations and the red broken line indicates the collapse time $\tau_c = 874$ years.* ***(b)*** *Annual mean MOC streamfunction pattern of equilibrium simulation 1.* ***(c)*** *Same as* ***(b)*** *but of equilibrium simulation 4.* ***(d)*** *Same as* ***(b)*** *but of equilibrium simulation 6.*

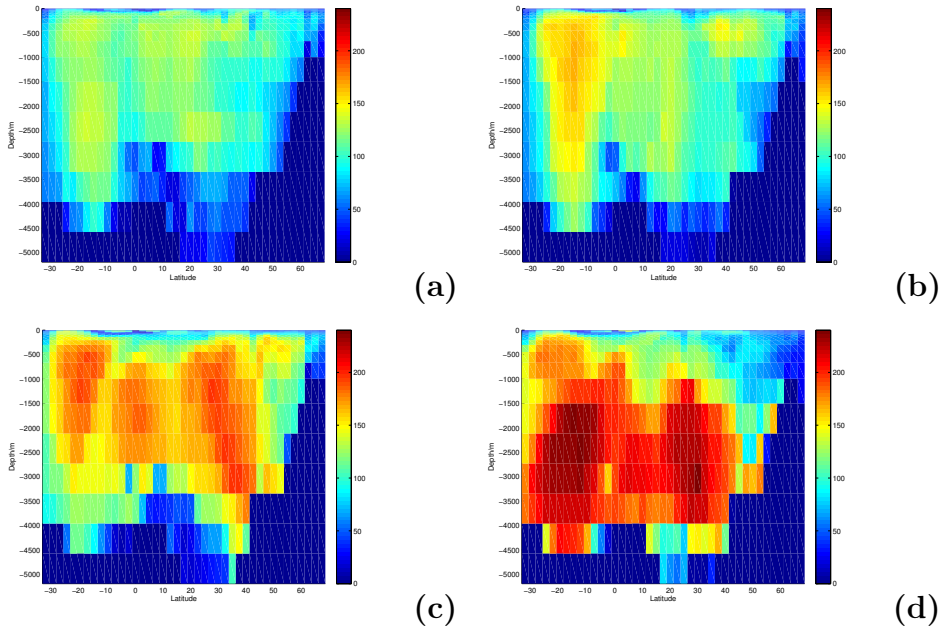

Figure 2: ***(a)*** *Degree field of the Pearson Correlation Climate Network (PCCN) constructed from the MOC data of equilibrium simulation 1 in Fig. 1****a*** *using a threshold* $\tau = 0.5$. ***(b)*** *Same as* ***(a)*** *but of equilibrium simulation 2.* ***(c)*** *Same as* ***(a)*** *but of equilibrium simulation 4.* ***(d)*** *Same as* ***(a)*** *of equilibrium simulation 6.*

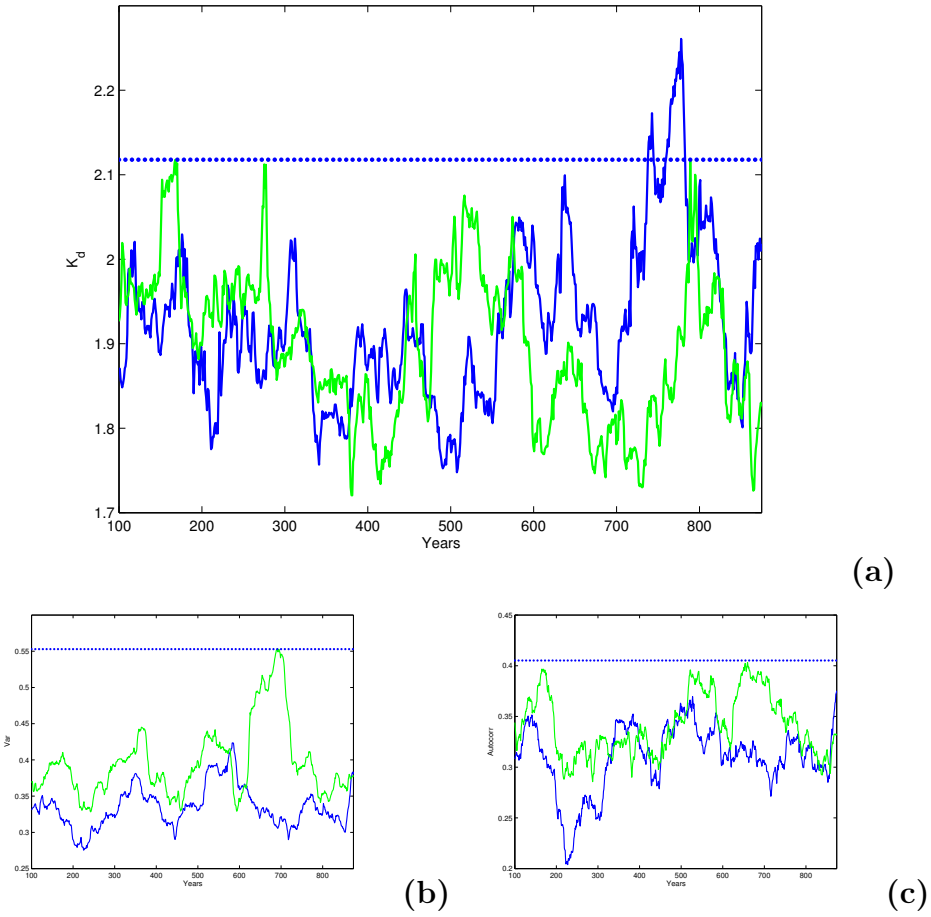

Figure 3: *For the complete Atlantic MOC field,* ***(a)*** *the kurtosis indicator K_d gives the early warning signal at 738 years and lasts for 44 years.* ***(b)*** *The traditional variance indicator Var gives no early warning signal before the collapse time $\tau_c = 874$ years.* ***(c)*** *The traditional lag-1 autocorrelation indicator Autocorr gives no early warning signal before the collapse time τ_c. Green solid curves are related to the control simulation and blue solid curves are related to the hosing simulation. The dashed blue horizontal lines indicate the corresponding maximum values of the control simulation.*

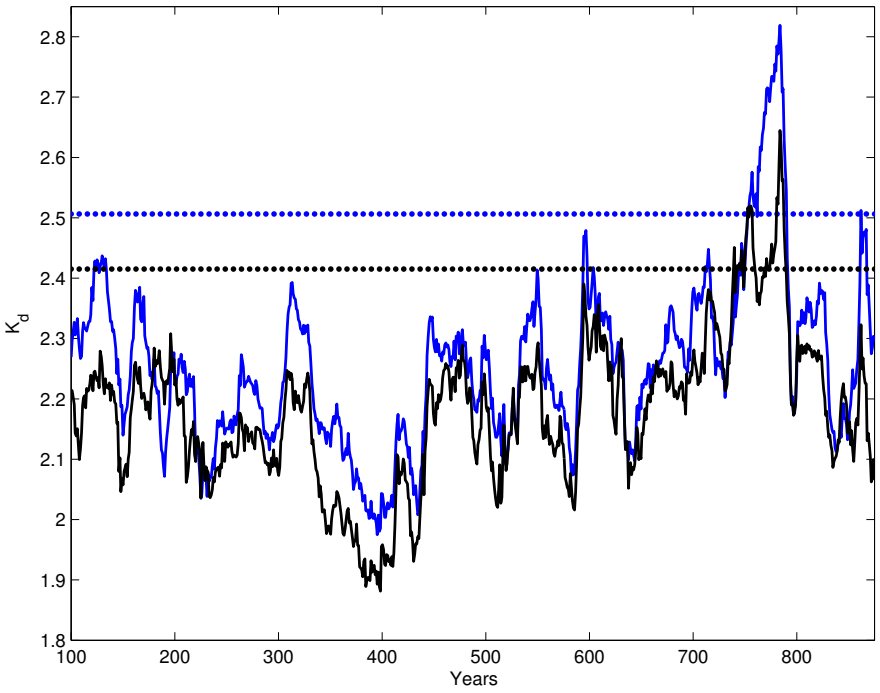

Figure 4: *The kurtosis indicator K_d for section data constructed from 21 depth levels and 8 latitudes.* ***(a)*** *Data from 31°N, 26°N, 21°N, 16°N, 11°N, 8°S, 13°S and 18°S (blue solid curve), gives the early warning signal at 753 years and lasts for 38 years.* ***(b)*** *Data from 31°N, 26°N, 21°N, 16°N, 11°N, 13°S, 18°S and 33°S (black solid curve), gives the early warning signal at 740 years and lasts for 49 years. The dotted blue horizontal line indicates the maximum K_d value of the control simulation of section data* ***(a)****, and the dotted black horizontal line indicates the corresponding maximum K_d value of section data* ***(b)****.*

Table 1: *The performance of the kurtosis indicator K_d based on complex networks constructed from sets of section data at different latitudes. In the sets of sections indicated by brackets, the first entry indicates the southern boundary, the second entry the northern boundary and the third entry is the latitudinal step.*

No.	Section	Detection Time (Year)	False Alarm	γ^{K_d}
1	(35°S, 70°N, 2.5°)	738	No	0.0675
2	26°N	384/567/868	Yes/Yes/No	0.1031/0.0451/0.0105
3	33°S	-	-	-0.1252
4	(35°S, 70°N, 5°)	739	No	0.0472
5	(20°N, 70°N, 5°)	-	-	0
6	(35°S, 20°N, 5°)	785	No	0.0559
7	(35°S, 35°N, 5°)	785	No	0.0773
8	(20°S, 35°N, 5°)	785	No	0.0584
9	Latitude set I	753	No	0.1248
10	Latitudes set II	740	No	0.0951
11	Latitude set III	-	-	-0.0810
12	Latitude set IV	-	-	-0.0454

I : 18°S, 13°S, 8°S, 11°N, 16°N, 21°N, 26°N and 31°N

II : 33°S, 18°S, 13°S, 11°N, 16°N, 21°N, 26°N and 31°N

III : 13°N, 16°N, 18°NS, 21°N, 23°N, 26°N, 28°N and 31°N

IV : 33°S, 31°S, 28°S, 26°S, 23°S, 21°S, 18°S and 16°S

arXiv:1405.1315v1 [physics.ao-ph] 6 May 2014

Supplementary Material to Deep Ocean Early Warning Signals of an Atlantic MOC Collapse

by

Qing Yi Feng, Jan P. Viebahn and Henk A. Dijkstra

This Supplementary Material contains the following:

1. Empirical Orthogonal Functions (EOFs) of the equilibrium MOC fields.
2. Performance of K_d, variance and autocorrelation indicators for single zonal sections.
3. Sensitivity of the K_d indicator to different section data.

1 The EOFs of the equilibrium MOC fields

From the 100 year MOC data of the equilibrium simulations of the FAMOUS model at the labelled points 1 - 6 in Fig. 1**a**, the EOFs were computed using standard methodology, which we repeat here for convenience. From the $n \times N$ (with $n = 100$ and $N = 21 \times 42 = 882$) data matrix F, ordered such that each column contains the MOC anomaly time series of a grid point, we form the $N \times N$ covariance matrix Σ by calculating

$$\Sigma = F^T F, \tag{1}$$

where the superscript T indicates the transpose. Next, we solve the eigenvalue problem

$$\Sigma \mathbf{e}_i = \lambda_i \mathbf{e}_i, \tag{2}$$

where the λ_i are the eigenvalues of Σ, with $i = 1, \cdots, N$ and the eigenvectors $\mathbf{e}_i$ are the EOFs.

The amount of variance σ_i explained by each EOF is obtained from

$$\sigma_i = \frac{\lambda_i}{\sum_{j=1}^{N} \lambda_j} \times 100\% \tag{3}$$

and the EOFs are typically ordered according to decreasing variance. Supplementary Fig. 1 shows the first EOF of each of the six different equilibrium simulations with the values of σ_i shown in the caption.

The first EOF becomes more dominant (i.e., the value of explained variance increases) when the freshwater forcing is increased (from 1 to 6). From Supplementary Fig. 1 one observes that for small freshwater forcing (panels **a**-**b**) most of the variability takes place near 15° and at about 1000 m depth. However, the maximum shifts to higher latitudes and deeper locations when the freshwater in increased (panels **c**-**e**) and closest to the transition (panel **f**) the maximum occurs at about 2000 m depth at both 20°S and 20°N.

The principal component (PC) time series of an EOF can be found by calculating

$$\mathbf{a}_i = F \mathbf{e}_i \tag{4}$$

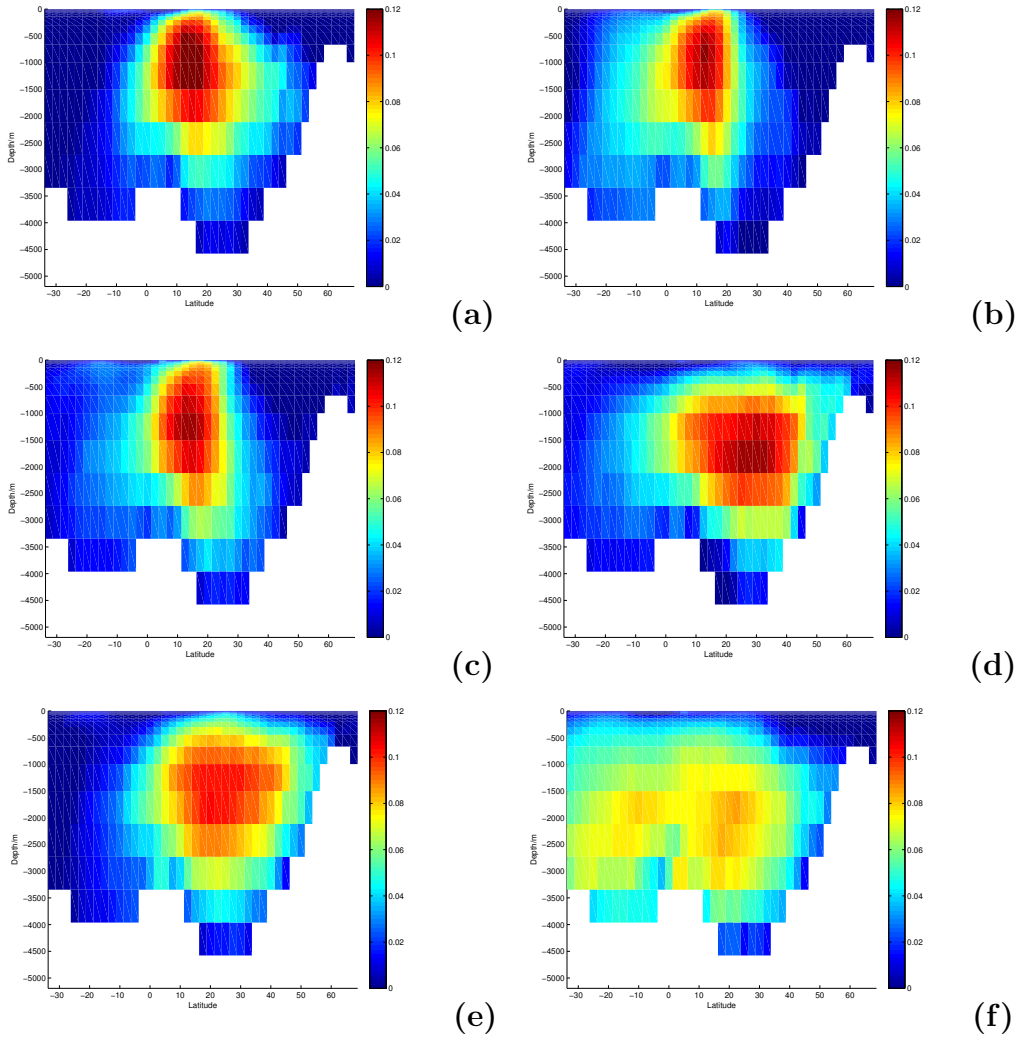

Supplementary Figure 1: ***(a)*** *The first EOF of the MOC data of equilibrium simulation 1, explaining 26.3% of the variance.* ***(b)*** *Same as* ***(a)*** *but of equilibrium simulation 2, explaining 24.1% of the variance.* ***(c)*** *Same as* ***(a)*** *but of equilibrium simulation 3, explaining 24.6% of the variance.* ***(d)*** *Same as* ***(a)*** *but of equilibrium simulation 4, explaining 37.1% of the variance.* ***(e)*** *Same as* ***(a)*** *but of equilibrium simulation 5, explaining 30.5% of the variance.* ***(f)*** *Same as* ***(a)*** *but of equilibrium simulation 6, explaining 37.6% of the variance.*

such that the data can be reconstructed from the EOFs and PCs by

$$F = \sum_{j=1}^{N} \mathbf{a}_j \mathbf{e}_j^T \tag{5}$$

This reconstruction can be used to determine how the different EOFs affect the degree distribution the network. For example, one can consider

$$F_1 = \mathbf{a}_1 \mathbf{e}_1^T \ ; \ F_2 = \mathbf{a}_1 \mathbf{e}_1^T + \mathbf{a}_2 \mathbf{e}_2^T \ ; \ F_3 = \mathbf{a}_1 \mathbf{e}_1^T + \mathbf{a}_2 \mathbf{e}_2^T + \mathbf{a}_3 \mathbf{e}_3^T \tag{6}$$

and reconstruct networks from each dataset F_i using the same methods described in the main text.

As all correlation coefficients for the dataset F_1 are unity, an interaction network based on F_1 is fully connected. The networks for F_2 and F_3 are not fully connected which indicates that as more EOFs explain the variance in the time series, the degree distribution deviates further from that of the maximum degree. This illustrates that when the tipping point is approached and one EOF tends to dominate in the time series, there will be regions of very high degree.

2 Performance of K_d, variance and autocorrelation indicators for single sections.

In Supplementary Table 1, we show the performance of the kurtosis indicator K_d constructed from 21 different single zonal sections. We excluded single sections north of 55°N as the MOC amplitude is very small here.

The performance of the variance indicator (Var) is shown in Supplementary Table 2. Obviously, the variance is not able to detect the MOC collapse because γ^{Var} is negative for each zonal section. The lag-1 autocorrelation (AC), shown in Supplementary Table 3, provides an early warning signal at a few zonal sections. However, the detection is either too early (false alarm) as for 21°N and 23°S or very late (as for 13°S).

Supplementary Table 1: *The performance of the kurtosis indicator K_d based on complex networks reconstructed from different single zonal sections*

Section	Detection Time (Year)	False Alarm	γ^{K_d}	Section	Detection Time (Year)	False Alarm	γ^{K_d}
33°S	-	-	-0.1252	11°N	-	-	-0.0202
28°S	-	-	-0.1540	16°N	872	No	0.1792
23°S	-	-	-0.0090	21°N	396/866	Yes/No	0.0045/0.0420
18°S	-	-	-0.0456	26°N	384/567/868	Yes/Yes/No	0.1031/0.0451/0.0105
13°S	-	-	-0.1774	31°N	384	Yes	0.0161
8°S	-	-	-0.0595	36°N	382	Yes	0.0909
3°S	-	-	-0.1937	41°N	586[(a)]	Yes	0.0057
1°N	-	-	0	46°N	-	-	-0.1463
6°N	-	-	-0.0840	51°N	-	-	-0.0260

(a) Signal only lasts for 2 years.

Supplementary Table 2: *The performance of the variance indicator Var at different single zonal sections*

Section	Detection Time (Year)	False Alarm	γ^{Var}	Section	Detection Time (Year)	False Alarm	γ^{Var}
33°S	-	-	-0.0694	11°N	-	-	-0.1505
28°S	-	-	-0.0697	16°N	-	-	-0.2153
23°S	-	-	-0.0747	21°N	-	-	-0.3104
18°S	-	-	-0.0868	26°N	-	-	-0.3773
13°S	-	-	-0.0500	31°N	-	-	-0.3389
8°S	-	-	-0.0515	36°N	-	-	-0.3116
3°S	-	-	-0.0326	41°N	-	-	-0.3482
1°N	-	-	-0.0402	46°N	-	-	-0.4464
6°N	-	-	-0.1279	51°N	-	-	-0.4735

Supplementary Table 3: *The performance of the Lag-1 Autocorrelation indicator AC at different single zonal sections*

Section	Detection Time (Year)	False Alarm	γ^{AC}	Section	Detection Time (Year)	False Alarm	γ^{AC}
33°S	-	-	-0.1470	11°N	-	-	-0.1168
28°S	-	-	-0.0265	16°N	-	-	-0.0512
23°S	497	Yes	0.0593	21°N	506	Yes	0.1769
18°S	-	-	-0.0987	26°N	-	-	-0.0471
13°S	870	No	0.0416	31°N	-	-	-0.0654
8°S	-	-	-0.0582	36°N	-	-	-0.0820
3°S	-	-	-0.0904	41°N	-	-	-0.0455
1°N	-	-	-0.0993	46°N	-	-	-0.1420
6°N	-	-	-0.0068	51°N	-	-	-0.1107

3 Sensitivity of the K_d indicator to different section data.

To further investigate the contribution of different sections to the detection of the MOC collapse, we exclude single sections one by one from the optimal locations we found (the set of eight sections labelled I in Table 1 in the main text), and evaluate the performance of the indicator K_d for the network reconstructed from the remaining seven locations.

As shown in Supplementary Table 4, sections 18°S and 31°N are essential for any detection. The data at sections 13°S and 8°S enhance the performance of the indicator K_d, by increasing the value of γ^{K_d}. The data at sections 11°N and 16°N prevent the occurrence of false alarms and the data at sections 21°N and 26°N decrease the detection time.

Supplementary Table 4: *Sensitivity test of the kurtosis indicator K_d by excluding, in each case, one single section from the set I of optimal sections given in Table 1 in the main text.*

Section	Detection Time (Year)	False Alarm	γ^{K_d}
7 latitudes (I−18°S)	-	-	-0.0303
7 latitudes (I−13°S)	768	No	0.0233
7 latitudes (I−8°S)	773	No	0.0047
7 latitudes (I−11°N)	596[(a)]/712[(b)]/772[(c)]	Yes/Yes/Yes	0.0175/0.0096/0.0163
7 latitudes (I−16°N)	443	Yes	0.1303
7 latitudes (I−21°N)	862	No	0.0977
7 latitudes (I−26°N)	859	No	0.0317
7 latitudes (I−31°N)	-	-	-0.0033

(a) Signal only lasts for 2 years.

(b) Signal only lasts for 1 years.

(c) Signal only lasts for 3 years.